Defect evolution in burnable absorber candidate material: Uranium diboride, UB$_2$

P.A. Burr [a, b, *], E. Kardoulaki [c], R. Holmes [b], S.C. Middleburgh [d, e]

[a] *School of Mechanical and Manufacturing Engineering, University of New South Wales, Kensington, 2052, NSW, Australia*
[b] *Australian Nuclear Science and Technology Organisation, Lucas Heights, 2234, NSW, Australia*
[c] *MST-8, Los Alamos National Laboratory, Los Alamos, NM, 87545, USA*
[d] *Nuclear Futures Institute, Bangor University, LL57 1UT, United Kingdom*
[e] *Westinghouse Electric Sweden AB, 72163, Västerås, Sweden*

ABSTRACT

The stability, diffusivity and clustering behaviour of defects in uranium diboride (UB$_2$) was investigated in light of the potential application as a burnable absorber in nuclear fuel. UB$_2$ was found to accommodate limited deviations from stoichiometry, which should be a consideration when manufacturing and operating the material. Self-diffusivity of both U and B was found to be sluggish (10^{-14} cm^2/s for B and 10^{-19} cm^2/s for U at 2000K) and highly anisotropic, with migration along the basal planes being orders of magnitude faster than *c*-axis migration. The anisotropy of defect migration (both interstitials and vacancies) is predicted to hinder recombination of defects produced by collision cascades, thus limiting the radiation tolerance of the material. Boron and uranium vacancies exhibit a drive to cluster. Boron vacancies in particular, which are mobile on basal planes, are predicted to cluster into strongly bound di-vacancy, which in turn are less mobile. These are then predicted to grow into larger two-dimensional vacancy clusters on the B plane, leading to anisotropic swelling. We provide an analytical expression to predict the stability of these clusters based on purely geometrical considerations. Finally, the accommodation of Li, He and Xe onto vacancy clusters was considered. Li appears to stabilise the structure upon U depletion, while the retention of He and Xe appears to rise with increasing B depletion, through the formation of vacancy clusters.

© 2018 Elsevier B.V. All rights reserved.

1. Introduction

Burnable absorbers are a widely utilised feature in nuclear fuels that can significantly improve the overall fuel cycle cost and extend residence times of fuel in a reactor. Burnable absorbers limit the reactivity of the fuel early on in the fuel's lifetime (by shielding portions of the fuel from thermal neutrons) allowing higher enrichment fuels to be loaded, thereby enabling a subsequent greater reactivity later on in the fuel bundle's cycle, once the burnable poison has been used.

1.1. Burnable absorbers

A widely used burnable absorbing material in the nuclear industry is gadolinia (Gd$_2$O$_3$) mixed into solid solution with the UO$_2$ fuel up to 10 wt% (normally 3—5 wt%). Gadolinium-157 has the highest thermal neutron cross section of any stable solid isotope in the periodic table (~242,000 b [1]). Gadolinium-155 also has a significant neutron cross section of ~56,000 b and can eventually absorb two neutrons to form [157]Gd. The multiple isotopes' behaviours results in a residual neutronic suppression, which is a drawback associated with Gd-based burnable absorbers using the natural isotopic abundances. Erbia has also been used as a burnable absorber in a similar manner and broadly behaves similarly to gadolinia [2].

Other thoroughly investigated consequences of adding gadolinia to UO$_2$ (in solid solution) include the reduction of fissile material from the assembly (as gadolinia displaces UO$_2$), a reduction in

---

* Corresponding author. School of Mechanical and Manufacturing Engineering, University of New South Wales, Kensington, 2052, NSW, Australia.
   E-mail address: p.burr@unsw.edu.au (P.A. Burr).

melting temperature of the fuel [3] and the significant degradation in thermal conductivity that the solid solution has in comparison with the fresh UO_2 material [4] (which also undergoes a significant reduction in thermal conductivity due to burnup effects [5]). Consequently, nuclear fuel manufacturers have pursued alternative burnable absorbing technologies: of note is the Integral Fuel Burnable Absorber (IFBA) technology developed by Westinghouse Electric Company using ZrB_2 [2,6,7].

Unlike Gd isotopes, there is only one stable highly neutron absorbing isotope of boron, B-10, which has a thermal neutron cross section of 3800 b [1]. Upon capture of a neutron, B-10 fissions into two very low thermal neutron cross section isotopes ^7Li and ^4He. The residual neutron poisoning of boron is therefore significantly lower than Gd.

Currently, IFBA is applied as a coating to the outside of the pellet due to manufacturing process restraints. However, the outer region of the pellet experiences significantly larger early burnup than in the centre of the pellet, causing the IFBA coating to burn away relatively quickly. In turn this leads to a peak in reactivity relatively early in the lifetime of the fuel, which limits the enrichment of the fuel in the assembly. This is highlighted by the blue line in Fig. 1.

By using UB_2 as an alternative to ZrB_2, and dispersing it as a second phase in UO_2, one can provide a suppressed initial fuel reactivity with a flater burnup dependence profile. As the uranium density of UB_2 is greater than UO_2, there will be more uranium in the pellet after the suppression of reactivity — effectively boosting the activity of the fuel later in the fuel cycle. To enable this technology, a significant effort in terms of experimental and theoretical understanding of UB_2 is required in relation to its potential use as a burnable absorber. In this work we aim to address the defect behaviour of UB_2, understanding the materials early behaviour in terms of radiation damage, defect migration, void nucleation and accommodation of fission and activation products.

1.2. Uranium diboride

Uranium diboride has a high melting point of 2430 °C [8] and high uranium density (11.68 g cm^{-3}), greater than that of UO_2 (9.67 g cm^{-3}). Theoretical studies have also reported that UB_2 exhibits an extraordinary thermal conductivity of 52 $Wm^{-1}K^{-1}$ in its un-irradiated state [9]. Experimental efforts have yielded a thermal conductivity of approximately a factor of two lower [10], which is still a remarkably high thermal conductivity.

UB_2 exhibits the AlB_2-type hexagonal structure (space group $P6/mmm$) [11], shown in Fig. 2. This phase is isostructural to many other metal diborides, that are known to exhibit extremely high melting point, hardness and thermal conductivity — properties
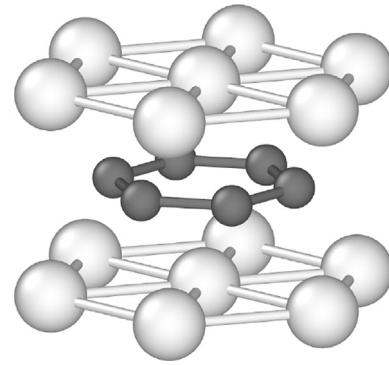

Fig. 2. Crystal structure of UB_2. Small dark spheres represent B atoms, and larger light spheres represent U atoms.

highly desired in advanced nuclear fuels. On the other hand, Th and Ce, which share many chemical similarities to U, do not form stable diborides [12]. Beckman and Kiessling suggest that because of the small atomic radius of B, the inter-atomic spacing of U atoms is suffciently small to promote metallic bonding with uranium layers [11], which would likely lead to a metallic-like thermal conductivity. This is not observed in the iso-structural β-USi_2 due to the larger Si radius [11].

Previous electronic structure calculations within the Density Functional Theory (DFT) framework investigated the nature of the chemical bonds and hybridisation within U−B compounds [13]. Recent DFT studies also considered some fission product behaviour in UB_2 [14] — highlighting that Zr and Xe cause contraction and swelling of the crystal structure respectively. Migration of defects through UB_2 was also studied: the U vacancy migration and concerted Xe/U-vacancy migration highlighted some initial fission gas release behaviour of the material. Electron density of states calculations have also shown that the material remains electrically conductive with increases in these extrinsic species in the UB_2 matrix.

2. Methodology

The density functional theory (DFT) simulations used in this work employed the plane-wave pseudo-potential VASP code [15,16] in conjunction with PAW pseudo-potentials [17]. The plane-wave cut-off was set to 400eV. The exchange-correlation functional used in this study is the PBE formalism of the generalised gradient approximation, and selected calculations were repeated with the hybrid HSE06 and PBE0 functionals.
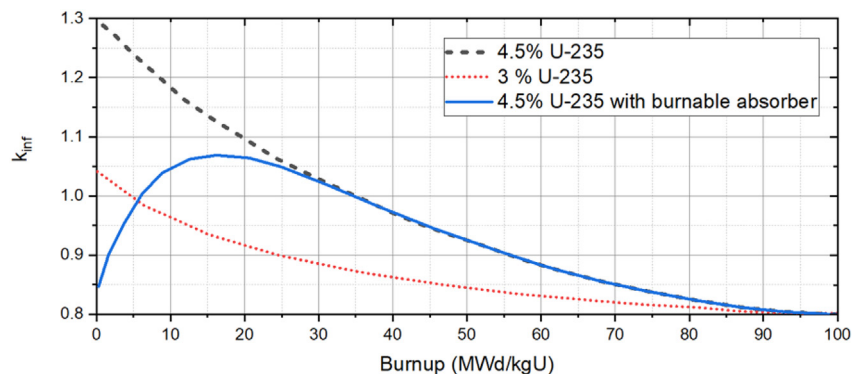

Fig. 1. Schematic showing reactivity (k_{inf}) of three different fuel designs: 4.5% enriched UO_2, 3% enriched UO_2 and 4.5% enriched UO_2 with ZrB_2 coated absorber highlighting its initial increase in reactivity. Modified from Ref. [2].

Crystal defects were investigated using supercells containing 144 atoms ($4 \times 4 \times 3$ expansion of the conventional unit-cell). Brillouin zone sampling was carried out using a $3 \times 3 \times 3$ Γ-centred k-point grid, equivalent to a k-point density of ~ 0.03 Å. In accordance with the semi-metallic nature of UB_2, first order Methfessel-Paxton [18] smearing of bands was employed with a width of 0.1 eV. Defect simulations were relaxed until the energy difference between two consecutive geometries was less than 1×10^{-4}eV.

Diffusion kinetics were calculated from harmonic transition state theory, informed by DFT calculations, with the aid of the "Onsager code" developed by Trinkle [19,20]. In the dilute limit, and for uncorrelated diffusion processes (i.e. tracer or self-diffusion), the diffusivity of a species A is simply related to the species concentration, c_A, and the respective diagonal Onsager transport coefficient L_{AA}

$$D_A = \lim_{c_A \to 0} \frac{k_B T}{c_A} L_{AA} \qquad (1)$$

Where a species may diffuse through both interstitial and vacancy-mediated mechanisms, D_A is the sum of the two diffusion mechanisms, each with the respective Onsager coefficient

$$D_A = c_A^i D_A^i + c_A^v D_A^v \qquad (2)$$

where c_A^i and c_A^v are the concentration of A interstitials and A vacancies respectively. Unlike extrinsic defect concentrations [21], the sum of $c_A^i + c_A^v$ is not a constant and may vary with temperature. The Onsager coefficients were calculated following transition state theory using a recently-developed numerical method based on Greens functions [19,20]. The activation energy for individual jumps were informed from DFT simulations using the nudged elastic band method with improved tangent [22] and climb image [23]. Pre-exponential factors (e.g. attempt frequencies) are known to be of secondary importance to the exponential term (energy barriers) [24,25], and hessian matrix calculations with the hopping atom approximation [24,26] show that for our system the difference in pre-exponential factor between ground state and transition state is negligible at the temperature of concern in this study.

This work was concerned with relatively large defect clusters, thus particular attention was taken to ensure that the supercell size was sufficiently large to avoid elastic self-interaction from periodic boundaries [27,28]. For every defect, the dipole tensor was calculated and the resulting self-interaction energy was consistently within 2% of the defect energy, owing to the strongly localised strain fields of the defects in this materials (see section 3.2). In addition, four defects (a single uranium vacancy, a single boron vacancy, a boron tetra-vacancy and a boron hexa-vacancy) were simulated in increasing supercell sizes from 54 to 216, showing convergence within 10^{-2}eV for supercells containing 96 atoms or more. As a final check, the difference between constant-pressure and constant-volume relaxation was computed for a uranium vacancy, and it was found to be <7 meV for supercells containing 144 atoms or more.

The behaviour of U and B intrinsic defects was computed as well as for extrinsic species: He, Li and Xe. Defect formation energies were used to understand the potential deviations in stoichiometry possible in UB_2 with respect to the uranium-rich and uranium-poor neighbouring phases U and UB_4. The binding energy of defect clusters was also computed to understand the interaction of different defects to each other in order to predict their resulting behaviour. Defect formation, binding and incorporation energies
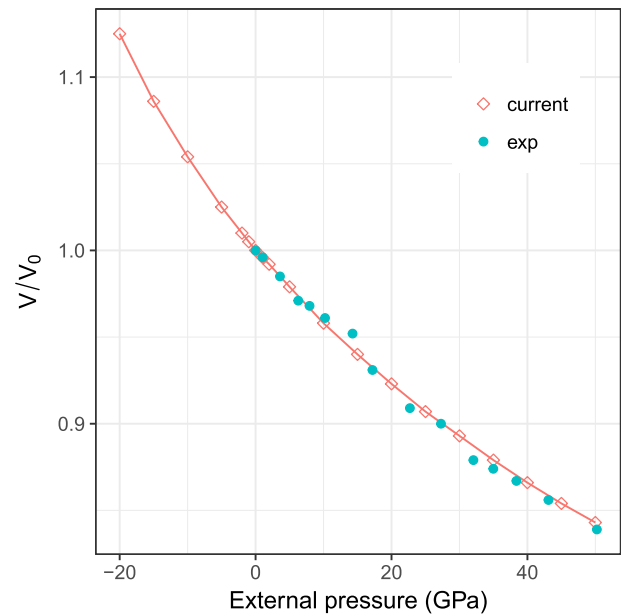

Fig. 3. Volume change as a function of applied hydrostatic pressure. Hollow symbols represent current DFT results and filled symbols were reproduced from experimental compression study [32].

were computed using established methods outlined in similar materials, see Appendix A for details and definitions.

Past work simulating UB_2 using DFT methods [9,14] has used an on-site Coulomb repulsion term '+U', also known as the Hubbard parameter. The magnitude of this parameter, and whether it is required at all, is entirely dependent on the material chemistry and crystal structure, and it is not transferable from one compound to a chemically similar but structurally different compound (or vice-versa, structurally similar but chemically different). Ideally, the U-value can be parameterised against photoemission spectroscopy experiments, see the exemplary case of UO_2 [29], or in the case of an insulator, it may be calculated self-consistently within the simulations with considerable success [30,31]. As there are no experimental information available regarding the electronic band structure of UB_2, and since the material does not have a band gap, it is impossible to infer a-priori what is a suitable Coulomb repulsion for this material. For reasons provided in Appendix B, we have chosen to omit an on-site Coulomb repulsion term for calculations presented in this body as benchmarking to lattice parameter alone does not provide sufficient justification for a correction term and the un-corrected results are shown to be in reasonable agreement with the body of experimental data available.

3. Results and discussion

3.1. Bulk properties

The response of UB_2 to hydrostatic compression was investigated experimentally by Dancausse et al. [32], and the pressure/volume curve is reproduced in Fig. 3 together with the current results from DFT, showing remarkable agreement between simulation and experiment.

The single-crystal elastic constants, c_{ij}, were calculated through perturbation theory and from these the polycrystalline bulk and shear moduli were obtained using a Hill average of the Reuss and Voight method [33]. These are presented in Table 1, and compared with previous DFT values of Jossou et al. [9] and experimental bulk

Table 1
Stiffness constants of UB_2 in units of GPa. Polycrystalline properties were calculated using the Voigt-Reuss-Hill averaging scheme 33.

	c_{11}	c_{33}	c_{12}	c_{13}	c_{44}	c_{66}	B	G
current (PBE)	444	502	71.5	104	263	186	216	213
experimental [32]							225 ± 2	
PBEsol [9]	342	503	161	280	105	90.4	275	87.9
PBEsol + U [9]	339	505	174	292	94.0	82.7	275	83.5

therefore low. This suggests that in the presence of excess boron or uranium (under equilibrium conditions) secondary phases are expected to form rather than the accommodation of deviations in stoichiometry — indicating that UB_2 is effectively a line compound. Compared to UO_2, which is able to accommodate significant variability in stoichiometry, UB_2 is expected to form secondary phases as boron or uranium is consumed through in-reactor processes.

CALPHAD analysis by Noordhoek and Besmann [36,37] has

Table 2
Intrinsic defect formation reactions in Kröger-Vink notation, normalised for unitary defects. Range of energies reported when multiple sites exist, see Appendix C for details on configuration, coordinates, energies and volumes of individual interstitial defects.

Defect	Reaction	Energy (eV/defect)	c (1000 °C)	c (2300 °C)
B-depletion (α-U, UB_2)				
V_B	$\frac{1}{2}\alpha - U + B_B \rightarrow V_B + \frac{1}{2}UB_2$	2.55	10^{-10}	10^{-6}
U_i	$\alpha - U \rightarrow U_i$	9.30–13.19	10^{-37}	10^{-20}
U_B	$\frac{3}{2}\alpha - U + B_B \rightarrow U_B + \frac{1}{2}UB_2$	6.02	10^{-24}	10^{-13}
B-excess (UB_2, UB_4)				
V_U	$UB_4 + U_U \rightarrow V_U + 2UB_2$	3.40	10^{-14}	10^{-8}
B_i	$\frac{1}{2}UB_4 \rightarrow B_i + \frac{1}{2}UB_2$	3.14–5.17	10^{-13}	10^{-7}
B_U	$\frac{3}{2}UB_4 + U_U \rightarrow B_U + \frac{5}{2}UB_2$	5.44	10^{-22}	10^{-12}
disorder				
B-Frenkel:	$B_B \rightarrow V_B + B_i$	3.10–4.12	10^{-12}	10^{-7}
U-Frenkel:	$U_U \rightarrow V_U + U_i$	7.29–8.67	10^{-29}	10^{-17}
Schottky:	$null \rightarrow V_U + 2V_B$	3.78	10^{-15}	10^{-09}
antisite:	$B_B + U_U \rightarrow B_U + U_B$	13.02	10^{-52}	10^{-28}

modulus of Dancausse et al. [32]. Despite the similarities in methodology between the two DFT studies,[1] there are remarkable differences for some of the stiffness constants, exemplified clearly by the varied shear constant values. Thus, the discrepancy provides an estimate of uncertainty of state-of-the-art DFT methods for UB_2 that can be reduced with eventual experimental efforts that will result if the concept outlined in this theoretical study is considered promising.

It is interesting to note that the bulk modulus is greater than the proposed parent material of the UB_2 burnable absorber — UO_2. The bulk modulus of UO_2 is approximately 210 GPa at room temperature [34,35] meaning that is more easily compressed in comparison to UB_2. Further work should address the potential burnup effects on the mechanical properties of UB_2 as well as radiation damage effects.

3.2. Defect behaviour and non-stoichiometry

To calculate the equilibrium concentration of defects, one must consider the formation of competing secondary phases, as presented in Table 2. Throughout the paper, when Kröger-Vink notation is used, it is implied that the defect in question is in UB_2. The concentrations were calculated for typical fuel operating temperature (1000 °C) and typical UB_2 sintering temperature of 2300 °C (for conventional pressureless sintering) — for details of all intrinsic defects and their formation energy in standard state, see Appendix C.

It can be seen that the energies are prohibitively high, and the corresponding concentrations at relevant temperatures are

shown that at equilibrium, composite formation of UO_2 and UB_2 leads to a slight reduction of the oxide to hypostoichiometric UO_{2-x}. This in itself is undesirable due to the reduction in melting point and thermal conductivity with hypostochiometry. The issue may be further aggravated during in-reactor operation, since the B depletion of the burnable poison leads to additional excess U that may not be entirely accommodated by the already hypostoichiometric UO_{2-x}, according to thermodynamic predictions [36]. If not accounted for, this may lead to the formation of metallic uranium, which is highly undesirable owing to its comparatively low melting temperature. Work should be carried out to identify the influence of fission product accommodation mechanisms in stoichiometrically varying UB_2 to fully appreciate the drive for secondary phase formation. This will enable work predicting the in-reactor behaviour of UB_2 that should consider not only the change in the parent material but also the change in behaviour due to the presence of any secondary phases (e.g. volume change, thermal conductivity and melting point).

As the next section deals with defect-defect interaction, it is important to note that dilute vacancies exhibit a strongly localised strain field with a marked anisotropic strain character. Atomic displacements (Fig. 4) on the nearest neighbours are remarkably
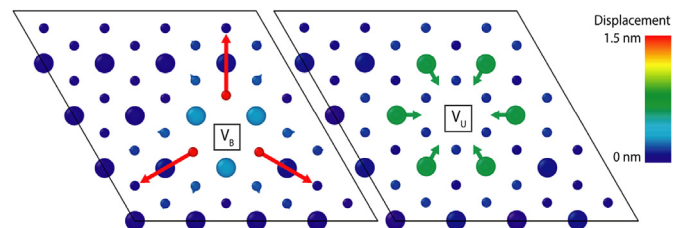
---

[1] Namely, two different formalisms of GGA exchange-correlation functional (PBE vs PBEsol), and different pseudo-potentials, which in turn is dictated by the fact that two different DFT codes were used.

Fig. 4. Strain fields of B and U vacancies. Arrows are scaled by a factor of 20 for clarity.

small (<1.5 nm), and negligible on all other atoms. The displacements are also restricted to in-plane neighbours only. This is consistent with the anisotropic elastic constant matrix (Table 1), dielectric tensor, and metallic-covalent nature of the material, which was reported to have covalent bond in plane and metallic bonds out of plane [9,13,38] (also evident in the charge density distribution of Fig. 5). Conveniently, this enables the study of reasonably large defect clusters (e.g. six-atom vacancy clusters) within a tractable supercell size (e.g. 144-atom supercell used in the current work).

3.3. Defect migration and self-diffusivity

The mobility of the point defects was investigated through CI-NEB calculations, combined with an Onsager diffusion analysis code [19,20]. Fig. 6 and Fig. 7 show the minimum energy pathway and resulting activation energy barrier for diffusion of vacancies and interstitials, respectively, within UB_2.

It is clear that vacancies (both V_U and V_B) exhibit markedly anisotropic diffusion, with basal migration being orders of magnitude faster than c-axis migration.

Interstitial diffusion (Fig. 7) is more complex as there are multiple paths that may lead to the equivalent final state: either a direct jump from an interstitial site a to a symmetrically equivalent interstitial site b; or a concerted motion of an interstitial from site a onto lattice site l while the atom originally on site l moves onto interstitial b. The latter is often referred to as the interstitialcy mechanism. Where appropriate, interstitialcy mechanisms were compared to direct interstitial diffusion mechanisms for both boron and uranium interstitial migration. Where a dumbbell configuration is involved (i.e. *1b-db* and *db-2c*) the jumps are identical for interstitial and interstitialcy mechanism.

Boron interstitial migration is found to be fastest in the basal plane: migrating with an energy of 1.3 eV. For jumps out of the basal plane, boron is required to overcome a significantly higher migration energy barrier of 2.25 eV — indicating boron interstitial diffusion is also highly anisotropic.

Uranium interstitial migration is more complex than that of boron interstitials due to the presence of more stable and metastable interstitial sites. Nevertheless, a jump network consisting exclusively of 3 g—2c jumps, with a relatively small migration energy of 1.3 eV, is sufficient to enable isotropic diffusion. Note that this jump includes two metastable intermediate states — these were relaxed in independent simulations and new NEBS were performed using the relaxed state as starting point. Despite the relatively low migration energy of uranium interstitials, their equilibrium concentration is so low (see Table 2) that the overall diffusivity of uranium interstitials is expected to be very low at equilibrium.
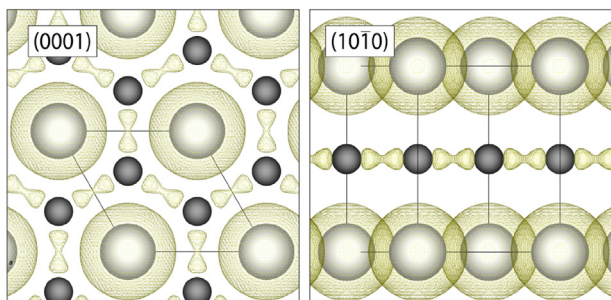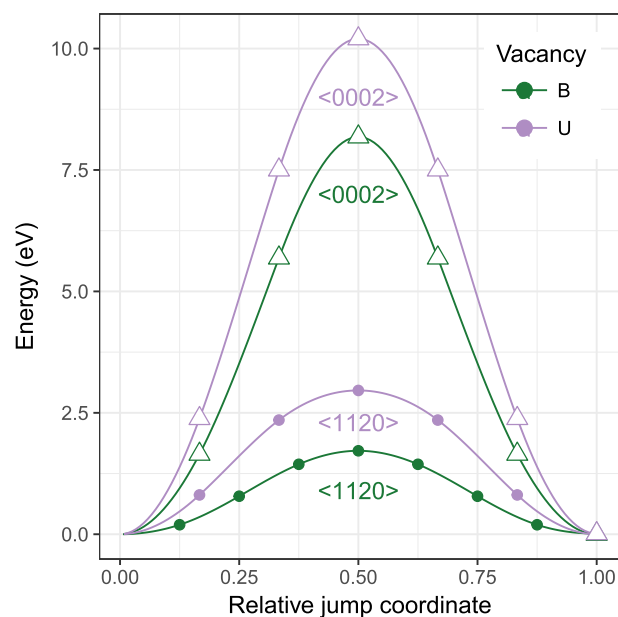

Fig. 6. Migration energy profile for V_U and V_B along the basal $\langle 1120 \rangle$ and c-axis $\langle 0002 \rangle$ directions.

Coupling all jumps together, it is possible to compute self-diffusivity, shown in Fig. 8. B self-diffusivity is dominated by interstitials and vacancies (in roughly equal measures) migrating on basal planes, while U self-diffusivity is orders of magnitude slower, and dominated by vacancy-mediated process (also limited to basal migration). Overall, all intrinsic species diffuse relatively slowly in UB_2. This is in line with the experimental observation that high temperatures are required to sinter UB_2 (~95% of melting point).

As the material shows significant anisotropic behaviour, any significant gradients in radiation damage in the material will result in significant deformation behaviour in a highly textured material. Differential radiation induced swelling, coupled with differential defect migration mechanisms may also lead to micro-cracking in poly-crystalline materials resulting in poor structural integrity after exposure to irradiation.

3.4. Clustering of defects

Vacancy clustering is now considered with a focus on the lowest energy (most favourable) intrinsic defect: the boron vacancy, as well as uranium vacancies that form as a result of Frenkel pair formation and Schottky defects. Clustering of vacancies, formed due to equilibrium or non-equilibrium processes, can lead to the formation of voids, which can cause swelling and degradation of bulk material properties.

The thermodynamic drive for vacancy clustering has been investigated by assessing the behaviour of increasing numbers of vacancies within a 144-atom supercell. Di-vacancies, both $\{V_B : V_B\}$ and $\{V_U : V_U\}$ as well as the mixed di-vacancy $\{V_U : V_B\}$ were considered, and their binding energies are presented in Fig. 9.

The clusters composed of $\{V_B : V_B\}$, $\{V_U : V_B\}$ and $\{V_U : V_U\}$ are found to have negative binding energies for most arrangements indicating they will bind to each other. The $\{V_B : V_B\}_{1nn}$ binding energy is particularly strong and may act as a nucleus for further vacancy clustering.

The kinetics of clustering of two boron vacancies was investigated by performing CI-NEB calculations of B vacancies migrating on the basal plane (Fig. 10). It is evident that there is no increase in
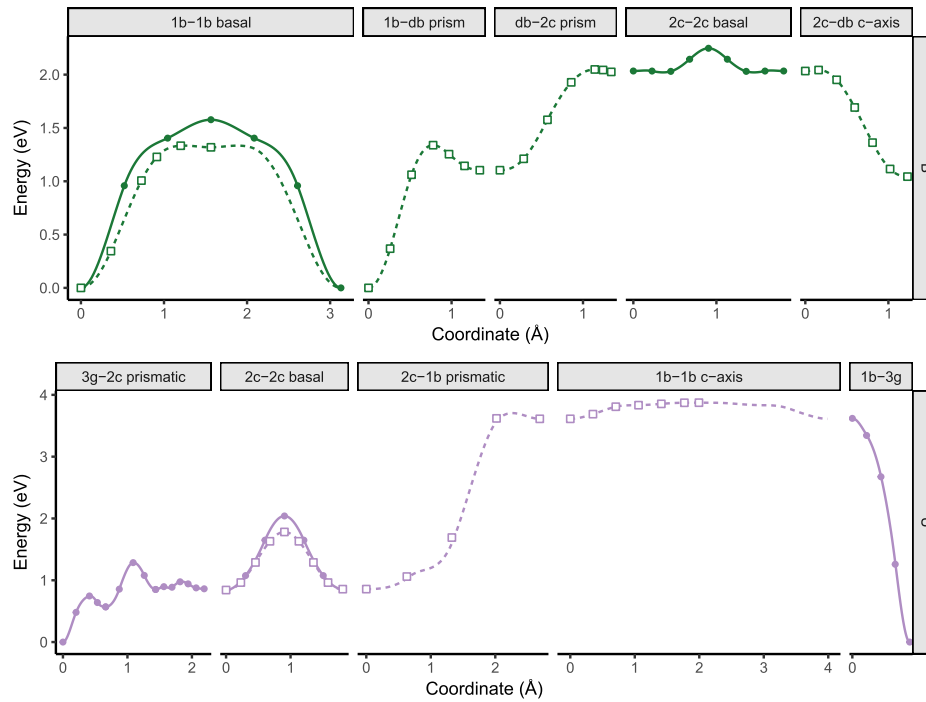

Fig. 5. Electronic density of UB_2. The isosurface represents a charge density of 0.115 electrons per voxel.

Fig. 7. Migration pathways of B and U self-interstitials. Dashed lines represent concerted migration (interstitialcy), solid line represent direct jumps. 'c-axis' and 'prismatic' refer to jump from boron to uranium planes, while 'basal' jumps refer to migration within planes of boron or uranium (for top and bottom panel respectively).
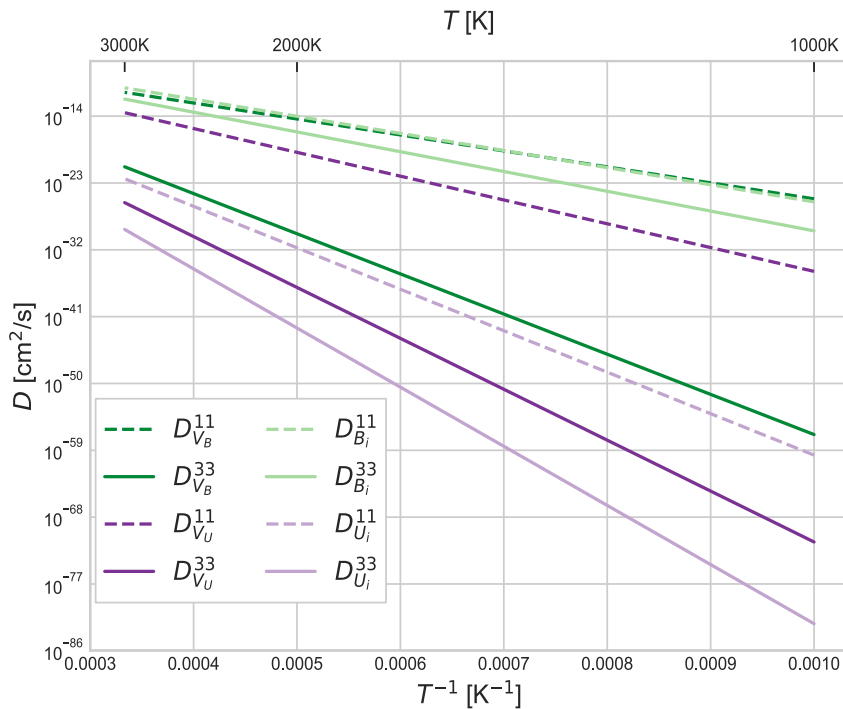

Fig. 8. Self diffusivity of B (green) and U (purple). Dashed lines represent basal diffusion, solid lines represent c-axis diffusion. Light and dark colours represent interstitial- and vacancy-mediated diffusion respectively. (For interpretation of the references to colour in this figure legend, the reader is referred to the Web version of this article.)

the defect diffusion barrier near the defect (i.e. there is no kinetic hindrance for vacancy clustering), on the contrary, there is a reduction in diffusion barrier from the 2nn to the 1nn configuration, whilst the barrier for the inverse process remains comparably large. Thus, if two boron vacancies fall within 3.04 Å of each-other,

they are highly likely to bind into the 1nn configuration, which is subsequently unlikely to dissociate. Since dissociation is a necessary step for the di-vacancy migration, this cluster is also predicted to be a comparatively slow diffuser.

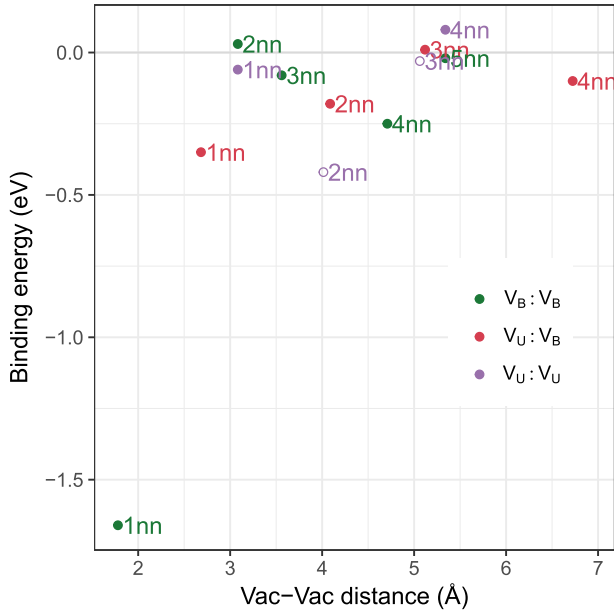Growth of the di-vacancy cluster into larger vacancy clusters,

Fig. 9. Binding energy of di-vacancy clusters as a function of inter-vacancy distance. Hollow points represent clusters where the vacancies are not within the same basal plane, or same UB$_2$ layer for $\{V_U : V_B\}$ clusters.

Fig. 10. Migration profile of boron di-vacancy clusters. Hollow triangles represent transition states and filled square represent binding energy of ground state di-vacancy configurations.
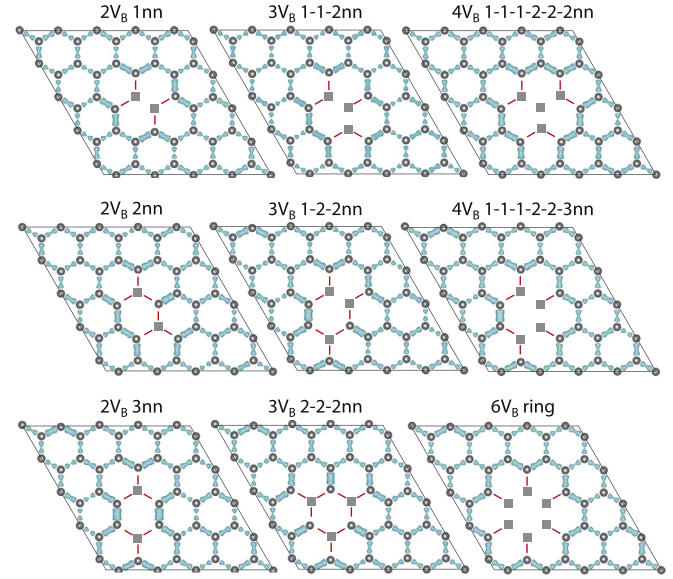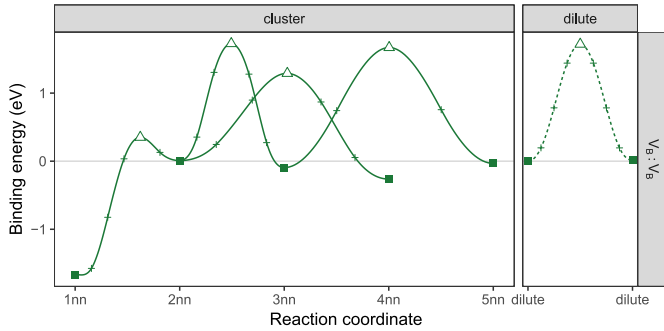

Fig. 11. Relaxed configurations and charge density of supercells containing planar V_B clusters. Turquoise isosurfaces represent charge densities of 0.116 electrons. Missing atoms and dangling bonds represented by grey squares and red lines respectively. Only one (0001) atomic layer is shown, projected from the c-axis. (For interpretation of the references to colour in this figure legend, the reader is referred to the Web version of this article.)

has been recorded in other layered and 2D materials such as boron nitride [39], graphite [40,41], graphene [42,43] and C-nanotubes [44,45].

Fig. 12b shows that this correlation between formation energy and the number of dangling bonds (both normalised by number of vacancies in the cluster) is linear. From this linear relationship, one can estimate the formation and binding energies of any planar V_B cluster of arbitrary size, as

$$E_f = n(1.148 + 0.738\,\delta)\ \text{eV} \tag{3}$$

$$E_b = n(-2.294 + 0.738\,\delta)\ \text{eV} \tag{4}$$

where n is the number of boron vacancies in the cluster, and δ is the number of dangling bonds per boron vacancy in the cluster. This surprisingly linear relationship enables the prediction of cluster stability simply based on a geometrical consideration, without having to perform computationally expensive DFT calculations, and can therefore be fed directly into larger scale models and fuel performance codes. Analogous relationships may be found in other layered and 2D materials in which vacancy clusters are known to re-arrange into lower energy configurations. Further work in these materials should consider the possibility of a linear relationship between cluster energy and number of dangling bonds.

3.5. Accommodation of activation and fission products

Absorption of thermal neutrons by boron-10 leads to the formation of He and Li, following the reaction:

$$^{10}\text{B} + n \rightarrow {}^{4}\text{He} + {}^{7}\text{Li} \tag{5}$$
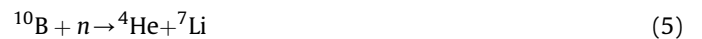
Thus it is important to understand how these are incorporated within the boride structure to predict the microstructural evolution with burn-up. In addition, uranium will also undergo fission, thereby producing fission products. Of particular importance is Xe, which is produced in large amounts and can have a significant

was considered. Starting from the strongly bound $\{V_B : V_B\}_{1nn}$ cluster, additional vacancies were added at varying distance from the di-vacancy cluster, all within the same basal plane. Example configurations are shown in Fig. 11. From the previous analysis on di-vacancies, as vacancies on different basal planes interact much more weakly (in line with the highly local and strongly isotropic strain field of a vacancy shown in Fig. 4), and as vacancies diffuse much faster along basal planes than across them, it is reasonable to only consider vacancies that are within the same basal plane.

Fig. 12a shows the formation energy (per vacancy) of the cluster as a function of cluster size. It is evident that all clusters are bound and the binding increase with increasing size. The colour coding illustrates how many "dangling bonds" are left behind in the material to form the cluster, clearly showing that the fewer dangling bond must be created to accommodate a vacancy, the lower the formation energy of the vacancy is. Thus, for any given cluster size, there is a strong driving force for re-arrangement into a configuration that leaves behind fewer dangling bonds. It is reasonable that no kinetic hindrance towards rearrangements exists, given the previous results on fast kinetics for V_B migration and $\{V_B : V_B\}$ rearrangement. Similar behaviour of in-plane vacancy rearrangement
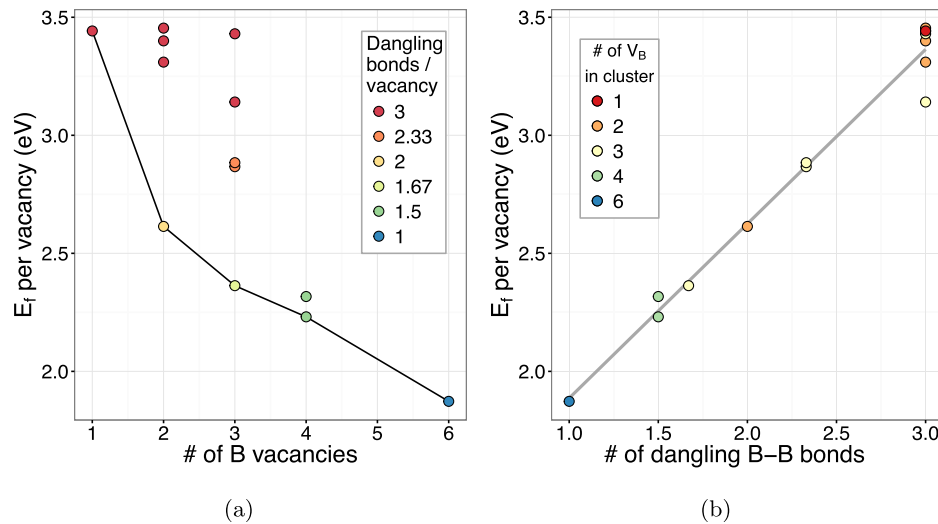
Fig. 12. Formation energy of planar V_B clusters normalised by the number of vacancies in each cluster.

impact on the thermal transport properties of a fuel and the swelling properties.

Here we consider the solubility of Li, He and Xe in pristine UB_2, and in the presence of vacancy clusters. The energy required to accommodate these extrinsic elements in the UB_2 crystal are shown in Fig. 13.

It is evident that interstitial sites are highly unfavourable for all species, in line with the relatively large atomic radii of these elements. Substitution onto B sites is also energetically unfavourable for all species, while substitution onto the U site is highly favourable for Li, and it may accommodate He relatively easily (0.71eV). It therefore appears that Li may act as a stabilising agent in UB_2 to compensate for U sub-stoichiometry due to fission.

The presence of pre-existing vacancy clusters, containing only V_B, significantly reduces the accommodation energy for all three species compared to single boron vacancies, with larger clusters providing the largest reduction. In the case of Xe, because of this progressive reduction in energy with increasing B vacancies, there

is no thermodynamic preference between accommodation onto a boron tri-vacancy or onto a U vacancy.

Given the universal preference for a U vacancy, we considered also clusters of V_B surrounding V_U. Interestingly, for the smaller atoms (He and Li), the addition of boron vacancies has no impact or even negative impact on their solubility. While for Xe, this results in additional reduction in energy, with a minimum observed for a Schottky cluster. The results suggest that retention of fission and activation products increases with increasing B depletion, which is promising since the rate of production of activation products is directly proportional with the rate of B depletion.

4. Summary

In this work, the intrinsic defect behaviour of UB_2 has been investigated in order to aid further studies understanding the behaviour of the ceramic operated as a component of nuclear fuel. It has been found that stoichiometry deviation is not easily accommodated within the structure and as such, any components manufactured from UB_2 would require significant stoichiometry control in order to avoid lower melting point phases (metallic U for example) or phases that may degrade the mechanical performance of the ceramic.

As the uranium or boron from the UB_2 is consumed by neutron absorption and fission, deviations in stoichiometry will vary accordingly. The presence of fission products (both from the U and the B reactions) may act to stabilise the structure; allowing deviations from stoichiometry to be accommodated. This requires further work using the methods outlined in this work.

The migration of vacancies in UB_2 was found to be highly anisotropic. As such, radiation damage processes will not easily anneal as defects from adjacent basal planes will not readily annihilate. Consequently, the radiation tolerance of UB_2 is expected to be lower than isotropic materials such as UO_2, despite the fact that the two compounds exhibit similar accommodation energies for disorder processes (Frenkel, anti-Frenkel, Schottkey and antisite disorder). Coupled with the anisotropy of vacancy migration, the activation energy for migration is also observed to be large, limiting the overall defect migration, further supporting a lack of defect recovery when exposed to displacive radiation environments.

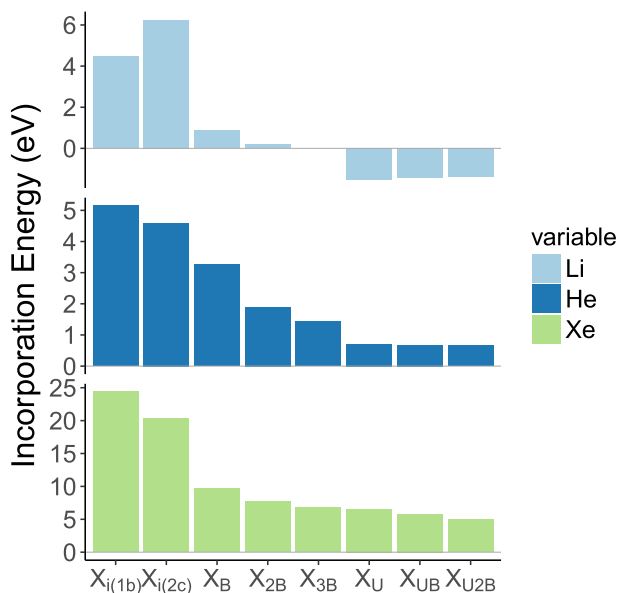Boron interstitials exhibit similar anisotropy and migration

Fig. 13. Incorporation energies of Li, He and Xe in UB_2.

barrier to boron vacancies. Uranium interstitials on the other hand diffuse isotropically through the material, and at a significantly faster rate than the corresponding vacancies.

Boron vacancies are relatively mobile on the basal planes and also exhibit a strong drive to cluster into strongly bound di-vacancies, and subsequently larger 2D vacancy clusters (on the basal plane). A fascinating outcome from the work is that the growth and stability of these clusters can be predicted based on the number of "dangling bonds" left as a result of the vacancy. It is expected that this behaviour will apply to a number of related compounds including the other layered diborides and potentially other highly covalent layered materials.

As the material is expected to accumulate defects quite readily in radiation environments, the volume change and anisotropic behaviour must be considered when designing fuels containing UB_2, for instance by providing sufficient porosity to accommodate swelling without imparting a significant outwards hoop strain on a cladding material. If used in small enough quantities within fuel, this swelling may be simply accommodated by careful consideration of the fuel-pellet gap size.

5. Data availability

The raw data required to reproduce these findings are available to download from https://doi.org/10.17632/42tc93n868.1.

Acknowledgments

Appendix A. Formation and binding energy definitions

The formation energy, E^f, of a defect is calculated as

$$E^f = E_{\text{def}}^{\text{DFT}} - E_{\text{perf}}^{\text{DFT}} \pm \sum_\alpha n_\alpha \mu_\alpha \tag{A.1}$$

where $E_{\text{def}}^{\text{DFT}}$ and $E_{\text{perf}}^{\text{DFT}}$ are the DFT total energies of the defective and pristine supercells (of same size), and μ is the chemical potential of all species α added or removed to form the defect. Under standard state conditions, the chemical potential is taken as the per-atom DFT energy of the element in its ground state. By way of example, the formation of a uranium vacancy in UB_2 is defined by the following reaction in Kröger-Vink notation

$$B_B \rightarrow V_B + \alpha - B(s) \tag{A.2}$$

The corresponding formation energy is calculated as

$$E_{B_U}^f = E_{V_B}^{\text{DFT}} - E_{B_B}^{\text{DFT}} + \mu_B \tag{A.3}$$

$$= E_{U_{48}B_{95}}^{\text{DFT}} - E_{U_{48}B_{96}}^{\text{DFT}} + \frac{1}{36}E_{\alpha-B_{36}(s)}^{\text{DFT}} \tag{A.4}$$

While the DFT energy of U and B in their elemental state provides an unequivocal definition of defect energy, and its self-consistency aids comparison across techniques, it does not reflect the conditions relevant to synthesis of this material or during reactor operations. In reality, when excess B is present, it precipitates in the form of UB_4, not α-B, as implicitly observed from the phase diagram. Thus, in this study we also report the formation energy considering the neighbouring stable phase in the U−B phase diagram as reservoir of chemical potential For instance, the same boron vacancy formation reaction in UB_2 under B-poor conditions is expressed as

$$\frac{1}{2}UB_2 + B_B \rightarrow V_B + \frac{1}{2}UB_4 \tag{A.5}$$

and the corresponding reaction energy is

$$E_{V_B}^{f(\text{B-poor})} = E_{U_{47}B_{96}}^{\text{DFT}} - E_{U_{48}B_{96}}^{\text{DFT}} + \frac{1}{2}E_{UB_4}^{\text{DFT}} - \frac{1}{2}E_{UB_2}^{\text{DFT}} \tag{A.6}$$

The binding energy of a defect cluster, E^b, is defined as the energy required to form the cluster from isolated non-interacting defects. It may be expressed in terms of formation energy of the constituent point defects i,

$$E^b = E_{\text{cluster}}^f - \sum_i E_i^f \tag{A.7}$$

With this definition, a positive binding energy denotes a repulsive interaction and a negative binding energy denotes an attractive interaction. The binding energy is independent on the chemical potential and the choice of formalism for E^f, since all terms of μ that appear in E_{cluster}^f must also appear in $\sum_i E_i^f$ and therefore cancel out.

The incorporation energy is defined as the energy penalty/gained to accommodate an extrinsic species X into a pre-existing defect

$$E^i(X) = E_{\text{defect}+X}^f - E_{\text{defect}}^f \tag{A.8}$$

as such, it is also independent on the chemical potential of U and B. The chemical potential of the He and Xe is taken from a DFT calculation of an isolated gas atom, and that of Li is taken from a DFT calculation of solid α-Li.

Appendix B. Exchange-correlation functional

Strongly correlated f-electron materials are typically not well simulated by the local density approximation and the generalised gradient approximation. Thus, it is customary to add an on-site Coulomb repulsion term '+U', also known as the Hubbard parameter. The parameterisation of this repulsive term poses a challenge: its purpose is to counters the spurious curvature of semi-local energy functionals as a function of electron occupation, whilst retaining the transferability of a "parameter-free" ab-initio approach [30]. Recently, Jossou et al. [9] performed DFT calculations of UB_2 with the PBEsol functional with a +U of 2eV, but they acknowledge that there is no ab-initio or experimental foundation to the choice of U value, but was simply treated as a empirical fitting parameter.

To assess the sensitivity of the results to the addition of a '+U', lattice parameters and formation energies of UB_2 were obtained for a range of U values from 0 to 6 eV at intervals of 0.1eV, as well as hybrid functionals HSE06 and PBE0 (with the conventional fraction of 0.25 Hartree-Fock exchange and, for HSE06, short range parameter $\omega = 0.2$). The results are presented in Figure B.14 and Table B.3.
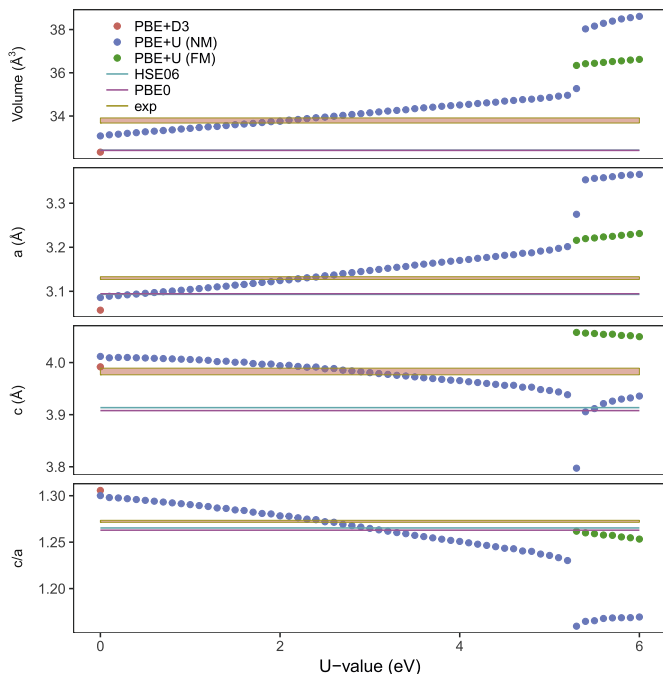
Fig. B.14. Lattice parameters of UB$_2$ as a function of +U. The width of red shades represent the 95% confidence interval on the spread of experimental data [11,12,32,46–50]. FM and NM represent ferromagnetic and non-magnetic calculations respectively. No FM calculations were stable with U < 5.3eV.

Table B.3 Enthalpy of formation of UB$_2$ in eV from different DFT methodologies and experiment 46.

exp 46	PBE	HSE06	PBE + D3	PBE + U (2 eV)
−1.690	−1.594	−1.968	−2.597	+0.261

It is evident that strongest alignment with experimental lattice parameters is found for U values in the range of 1.8eV–3.2eV, in line with Jossou et al. [9] choice of $U = 2.0$ eV — although note that the exchange-correlation functional and the pseudopotentials are also different between the two studies. However, it is also evident that at no value of U can we reach agreement with both experiments and hybrid calculations, which reduces the confidence on the need for an on-site Coulomb repulsion. Notably, an excessive Coulomb repulsion (U > 5.3 eV) leads to the stabilisation of a ferromagnetic state, which is not observed with the hybrid or PBE functionals, and for which there is no experimental evidence. The addition of the '+U' term also requires careful treatment of the formation energies (of bulk phases and of defects) to counter the spurious positive energy term caused by on-site Coulomb repulsion, typically by empirical alignment with experimental data [51,52]. Without such empirical correction, the formation energy of UB$_2$ becomes positive, which is unphysical for a stable phase.

On the other hand, when no on-site Coulomb repulsion is used, the DFT lattice parameters and formation energies are within ±1.5% and 6% of the experimental average, which is within the typical range of uncertainty of PBE calculations, again suggesting that the on-site Coulomb repulsion may not be necessary. Similarly good agreement is found for the elastic properties (see section 3.1). Furthermore, Yamamoto et al. [53] have performed low-temperature field modulation de Haas-vanAlphen oscillation measurements on single crystal UB$_2$ and found that the electronic structure is well represented even within the linear density

approximation (LDA). Thus, to prevent additional uncertainty arising from arbitrary choice of U value, the calculations of the current work were performed with the PBE functional without an on-site Coulomb repulsion.

Appendix C. Details of intrinsic defects

Details of the stable intrinsic point defects is provided in Table C.4. For ease of comparison with other computational and experimental work, we report the formation energy from standard state, E_f°, in which the chemical potential of the atoms added or removed to form the defect is taken from reservoirs of elemental metals in their standard state (i.e. α-B$_{(s)}$ and α-U$_{(s)}$). The relaxation volume, Ω, is defined as the change in volume between the defective and pristine supercells, and was obtained from the elastic dipole of the relaxed defect and the material's elastic constant (see Table 1), following linear elastic theory.

Table C.4
List of stable intrinsic point defects in UB$_2$, together with the Wyckoff site, atomic coordinate in the conventional unit cell, the formation energy in standard state and relaxation volume. In addition, two metastable sites were observed for U$_i$ between the 3g and the 2c sites, with formation energies of 9.87eV and 10.13eV.

Name	defect type	site	coordinates	E_f° (eV)	Ω
V_B	vacancy	2d	$\left(\frac{1}{3}, \frac{2}{3}, \frac{1}{2}\right)$	3.45	−0.58
V_U	vacancy	1a	$(0,0,0)$	4.43	−5.08
$B_{i(1b)}$	interstitial	1b	$\left(0, 0, \frac{1}{2}\right)$	2.75	8.10
$B_{i(2c)}$	interstitial	2c	$\left(\frac{2}{3}, \frac{1}{3}, \frac{1}{2}\right)$	4.79	9.26
$B_{c-dumbbell}$	interstitial	4h	$\left(\frac{1}{3}, \frac{2}{3}, 0.307\right)$	4.09	9.24
$B_{a-dumbbell}$	interstitial	12q	$(0.1182, 0.3878, 0)$	3.83	11.19
$B_{p-dumbbell}$	interstitial	12o	$(0.38, 0.62, 0.6)$	3.87	10.48
$U_{i(3g)}$	interstitial	3g	$\left(\frac{1}{2}, \frac{1}{2}, \frac{1}{2}\right)$	9.30	26.31
$U_{i(2c)}$	interstitial	2c	$\left(\frac{2}{3}, \frac{1}{3}, \frac{1}{2}\right)$	10.15	29.60
$U_{i(1b)}$	interstitial	1b	$\left(0, 0, \frac{1}{2}\right)$	12.92	37.41
$U_{c-dumbbell}$	interstitial	2e	$(0,0,0.280)$	11.09	40.97
$U_{a-dumbbell}$	interstitial	6l	$(0.448, 0.224, 0)$	13.19	31.10
B_U	substitution	1a	$(0,0,0)$	6.09	−4.98
U_B	substitution	2d	$\left(\frac{1}{3}, \frac{2}{3}, \frac{1}{2}\right)$	6.93	20.01

References

[1] V.F. Sears, Neutron News 3 (1992) 26–37.
[2] F. Franceschini, B. Petrović, Ann. Nucl. Energy 36 (2009) 1201–1207.
[3] S.G. Popov, V. a. Lysenko, V.N. Proselkov, High Temp. 50 (2012) 221–224.
[4] M. Hirai, S. Ishimoto, J. Nucl. Sci. Technol. 28 (1991) 995–1000.
[5] M.J. Qin, M.W.D. Cooper, E.Y. Kuo, M.J.D. Rushton, R.W. Grimes, G.R. Lumpkin, S.C. Middleburgh, J. Phys. Condens. Matter : Inst.Phys. J. 26 (2014) 495401.
[6] S.C. Middleburgh, D.C. Parfitt, P.R. Blair, R.W. Grimes, J. Am. Ceram. Soc. 94 (2011) 2225–2229.
[7] R.L. Simmons, N.D. Jones, F.D. Popa, D.E. Mueller, J.E. Pritchett, Nucl. Technol. 80 (1988) 343–348.
[8] L. Brewer, D.L. Sawyer, D.H. Templeton, C.H. Dauben, LBNL Report # UCRL-603, 1950.
[9] E. Jossou, L. Malakkal, B. Szpunar, D. Oladimeji, J.A. Szpunar, J. Nucl. Mater. 490 (2017) 41–48.
[10] E. Kardoulaki, K.J. McClellan, Personal Communication, 2017.
[11] G. Beckman, R. Kiessling, Nature (1956) 1341.
[12] F.A. Rough, A.A. Bauer, Constitution of Uranium and Thorium Alloys, Technical Report, Battelle Memorial Institute, Columbus, Ohio, 1958.
[13] S.F. Matar, J. Etourneau, Int. J. Inorg. Mater. 2 (2000) 43–51.
[14] E. Jossou, D. Oladimeji, L. Malakkal, S. Middleburgh, B. Szpunar, J. Szpunar, J. Nucl. Mater. 494 (2017) 147–156.
[15] G. Kresse, J. Furthmüller, Phys. Rev. B 54 (1996) 11169–11186.
[16] G. Kresse, Comput. Mater. Sci. 6 (1996) 15–50.

[17] G. Kresse, D. Joubert, Phys. Rev. B 59 (1999) 1758−1775.
[18] M. Methfessel, A. Paxton, Phys. Rev. B 40 (1989) 3616−3621.
[19] D.R. Trinkle, Phil. Mag. 97 (2017) 2514−2563.
[20] D.R. Trinkle, Phil. Mag. 96 (2016) 2714−2735.
[21] P.A. Burr, M.R. Wenman, B. Gault, M.P. Moody, M. Ivermark, M.J.D. Rushton, M. Preuss, L. Edwards, R.W. Grimes, J. Nucl. Mater. 467 (2015) 320−331.
[22] G. Henkelman, H. Jónsson, J. Chem. Phys. 113 (2000) 9978−9985.
[23] G. Henkelman, B.P. Uberuaga, H. Jónsson, J. Chem. Phys. 113 (2000) 9901−9904.
[24] L. Messina, M. Nastar, N. Sandberg, P. Olsson, Phys. Rev. B 93 (2016) 184302.
[25] P.A. Burr, S.X. Oliver, J. Eur. Ceram. Soc. (2018). https://doi.org/10.1016/j.jeurceramsoc.2018.10.001.
[26] T. Garnier, V.R. Manga, P. Bellon, D.R. Trinkle, Phys. Rev. B 90 (2014) 24306.
[27] C. Varvenne, F. Bruneval, M.-C. Marinica, E. Clouet, Phys. Rev. B 88 (2013) 134102.
[28] P.A. Burr, M.W.D. Cooper, Phys. Rev. B 96 (2017) 094107.
[29] B. Dorado, M. Freyss, B. Amadon, M. Bertolus, G. Jomard, P. Garcia, J. Phys. Condens. Matter 25 (2013) 333201.
[30] M. Cococcioni, S. de Gironcoli, Phys. Rev. B 71 (2005) 1−16.
[31] H.J. Kulik, M. Cococcioni, D.A. Scherlis, N. Marzari, Phys. Rev. Lett. 97 (2006) 1−4.
[32] J.-P. Dancausse, E. Gering, S. Heathman, U. Benedict, L. Gerward, S. Staun Olsen, F. Hulliger, J. Alloy. Comp. 189 (1992) 205−208.
[33] R. Hill, Proc. Phys. Soc. (1952) 349−354.
[34] J. Wachtman, M. Wheat, H. Anderson, J. Bates, J. Nucl. Mater. 16 (1965) 39−41.
[35] I.J. Fritz, J. Appl. Phys. 47 (1976) 4353−4358.
[36] M.J. Noordhoek, T.M. Besmann, Thermodynamic Analysis of Select Composite Nuclear Fuels, Technical Report, University of South Carolina, 2015.
[37] K. McClellan, FY2015 Ceramic Fuels Development Annual Highlights, Technical Report, Los Alamos, NM, USA, 2015.
[38] X. Chen, Q. Tu, M. He, L. Dai, L. Wu, J. Phys. Condens. Matter 13 (2001) L723−L727.
[39] S. Okada, Phys. Rev. B Condens. Matter 80 (2009) 1−4.
[40] A. El-Barbary, H. Telling, P. Ewels, I. Heggie, R. Briddon, Phys. Rev. B Condens. Matter 68 (2003) 1−7.
[41] Z. Tang, M. Hasegawa, T. Shimamura, Y. Nagai, T. Chiba, Y. Kawazoe, M. Takenaka, E. Kuramoto, T. Iwata, Phys. Rev. Lett. 82 (1999) 2532−2535.
[42] F. Banhart, J. Kotakoski, A.V. Krasheninnikov, ACS Nano 5 (2011) 26−41.
[43] M. Saito, K. Yamashita, T. Oda, Jpn. J. Appl. Phys. Part 2: Lett. 46 (2007) 1185−1187.
[44] J. Kotakoski, A.V. Krasheninnikov, K. Nordlund, Phys. Rev. B Condens. Matter 74 (2006) 1−5.
[45] J.E. Padilha, R.G. Amorim, A.R. Rocha, A.J.R. Da Silva, A. Fazzio, Solid State Commun. 151 (2011) 482−486.
[46] H.E. Flotow, J. Chem. Phys. 51 (1969) 583.
[47] A.M. Mulokozi, J. Less Common. Met. 71 (1980) 105−111.
[48] L. Toth, H. Nowotny, F.B.E. Rudy, Monatshefte für Chemie und verwandte Teile anderer Wissenschaften 92 (1961) 794−802.
[49] L. Brewer, D.L. Sawyer, D.H. Tempelton, C.H. Dauben, J. Am. Ceram. Soc. 34 (1951) 173−179.
[50] J.L. Lunsford, R.J. Fries, C.P. Kempter, Crystal Front 2 (1961).
[51] V. Stevanović, S. Lany, X. Zhang, A. Zunger, Phys. Rev. B 85 (2012) 1−12.
[52] A. Jain, G. Hautier, S.P. Ong, C.J. Moore, C.C. Fischer, K.A. Persson, G. Ceder, Phys. Rev. B 84 (2011) 1−10.
[53] E. Yamamoto, Y. Haga, T. Honma, Y. Inada, D. Aoki, M. Hedo, Y. Yoshida, H. Yamagami, Y. Onuki, J. Phys. Soc. Jpn. 67 (1998) 3171−3175.